Contact Analysis of Functionally Graded Carbon Nanotubes Reinforced Composite (FG-CNT)

Rakesh Bhadra, Tamonash Jana, Anirban Mitra, and Prasanta Sahoo

Abstract The primary focus of this study is to examine how the arrangement of carbon nanotubes (CNTs) within a functionally graded nanocomposite (FG-CNT) impacts its behavior. A finite element model for contact, based on spherical indentation, is created using APDL code within the ANSYS platform. The analysis involves three different distribution patterns: uniform distribution (FG-UD), distribution with decreasing order (FG-V), and distribution with increasing order (FG-Λ) from the contact surface toward the base. The model's accuracy is confirmed by comparing its results with existing literature. Key parameters such as contact force, contact area, stress distribution, and deformation characteristics are extracted from the contact model. Through a detailed investigation, it is found that the FG-V distribution pattern exhibits enhanced contact properties.

Keywords Carbon nanotubes · Nanocomposites · FG-CNT · FEM · Indentation contact simulation

1 Introduction

In contemporary engineering applications, Functionally Graded Materials (FGMs) have gained widespread acceptance and application across various domains, including tribology, biomechanics, nanotechnology, sensor technology, thermal barrier coatings for turbine blades, and optical/electrical applications [1]. The popularity of FGMs is attributed to their exceptional thermal and mechanical properties,

R. Bhadra (✉) · T. Jana · A. Mitra · P. Sahoo
Department of Mechanical Engineering, Jadavpur University, Kolkata 700032, India
e-mail: rakeshbhadra20@gmail.com

R. Bhadra
Department of Mechanical Engineering, Tezpur University, Sonitpur 784028, India

T. Jana
Department of Mechanical Engineering, Institute of Engineering and Management (IEM), University of Engineering and Management, Kolkata 700091, India

P. Sahoo and T. K. Barman (eds.), *Advances in Materials, Manufacturing and Design*, Lecture Notes in Mechanical Engineering,
https://doi.org/10.1007/978-981-97-6667-3_59

improved interfacial bonding attributes, reduced stress concentration, and heightened resistance to fracture initiation [2]. Given these properties, there is a growing need to explore the contact behavior of FGMs and its associated materials, and this study focuses on employing indentation techniques to understand such behavior.

Shen and Zhang [3] analyzed thermal buckling and post-buckling responses in an FG-CNT flat panel using thin-beam theory (TBT) and von-Karman geometric nonlinearity, employing panel thickness significantly smaller than other dimensions and substantial deflections affecting curvature. Shen and Xiang [4] extended this study to nonlinear bending, vibration, and post-buckling of an FG-CNT beam on elastic foundations, utilizing higher-order shear deformation theory (HSDT) to consider shear deformations. Shiau and Kuo [5] explored thermal buckling in a sandwich panel via first-order shear deformation theory (FSDT), suitable for simpler engineering applications compared to HSDT. Zhu et al. [6] used FSDT to examine free vibration and bending of an FG-CNT plate, revealing carbon nanotube volume's significant impact on plate frequencies. Shen [7] analyzed the thermal post-buckling of CNT-reinforced composite cylindrical shells, combining HSDT and von-Karman nonlinear kinematics, emphasizing boundary conditions and shell thickness effects. Yas and Samadi [8] studied functionally graded CNT-reinforced composite panels' vibration and buckling using TBT. Mehrabadi et al. [9] investigated functionally graded SWCNT-reinforced flat panel buckling via FSDT. Kerur and Ghosh [10] explored nonlinear transient behaviors in composite panels with active fiber composites and PVDF layers, utilizing FSDT.

Bhadra et al. [11–13] numerically established the contact behavior of CNT-based nanocomposites comprising CNTs and elastoplastic materials in their research, considering frictionless contact. Baltacıoğlu et al. [14] conducted vibration analysis on an FG-CNT nanocomposite to identify the effect of CNT distribution in the nanocomposite. Yadav et al. [15] conducted a thermally induced fracture analysis on carbon nanotube (CNT)-reinforced functionally graded (FG) structures. The study focused on investigating the influence of varying CNT percentages on the properties of CNT-reinforced FG composites. Lei et al. [16] studied FG-CNT cylindrical panel-free vibration with FSDT shell theory, employing the element-free Galerkin method. Literature reveals extensive research into the vibration and deflection behavior of FG-CNT nanocomposites, though limited attention is given to analyzing contact phenomena within FG-CNT nanocomposites.

The current investigation addresses the above-mentioned research gap by primarily adopting an indentation-based approach. The loading–unloading process is simulated by implementing downward and upward displacement of a rigid spherical indenter within the 3D Finite Element Model (FEM). The distribution of carbon nanotubes (CNTs) in the matrix material follows various configurations, such as FG-UD, FG-V, and FG-Λ. The analysis focuses on extracting various contact parameters (contact force, contact area, stress distribution, and deformation characteristics). These parameters collectively contribute to identifying the maximum extent of contact attributes within the FG-CNT nanocomposites.

2 Finite Element Modeling

The present study analyses single asperity indentation contact between a rigid spherical indenter and functionally graded nanocomposite, where, the distribution of the CNTs is as per different patterns. The pattern in the distribution provides the functional gradation of properties. The model is implemented using ANSYS finite element software and consists of three phases: Aluminum (Al) as the matrix material, CNT distribution as the reinforcement material with specific distribution patterns, and a rigid spherical indenter. The FE model of the contacting system is shown in Fig. 1.

The model's coordinate system (Fig. 1) considers the y-axis as the vertical axis, while the x–z plane defines the base of the model. To reduce computation time, half of the model is analyzed, with the x–y plane serving as the plane of bisection. The nanocomposite comprises CNT-Al with specific distribution of the nanotubes, and material properties for Al and CNT include elastic–plastic behavior with bilinear isotropic hardening in the post-elastic regime. The von Mises yield criterion is applied in the plastic-yield region. Three CNT distribution patterns (Fig. 2)—uniform (UD), increasing from the contact surface (Λ), and decreasing from the contact surface (V)—are considered to ascertain the effect of different patterns on the contact behavior.

The nanocomposite's dimensions are 50 nm × 30 nm × 25 nm, with CNTs having an outer radius of 1.50 nm and a thickness of 0.34 nm. CNTs are assumed to

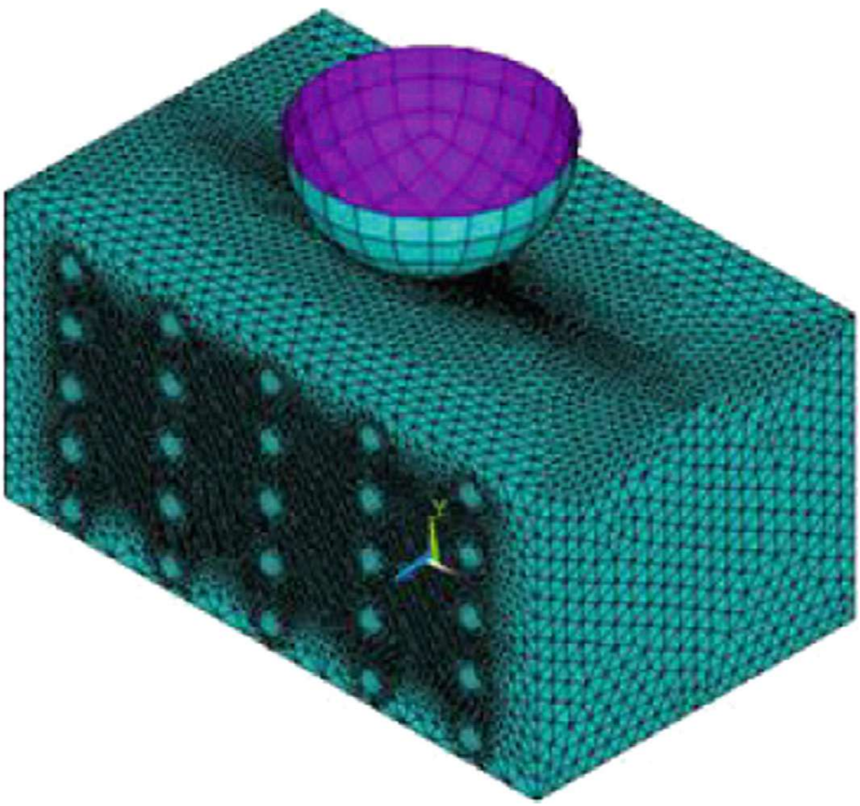

Fig. 1 Finite element model and mesh of the contact interface

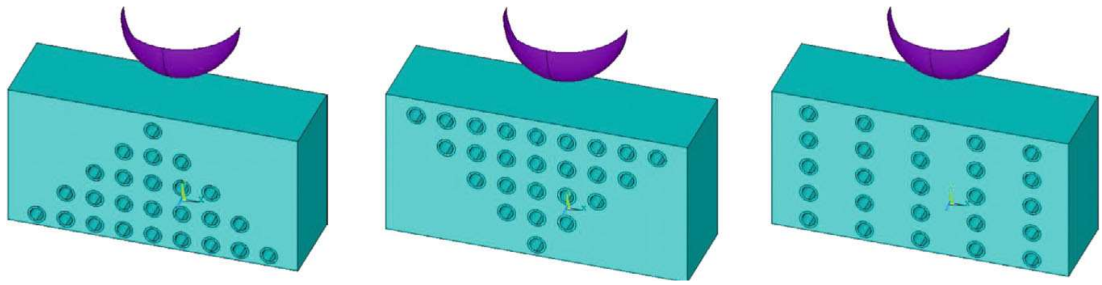

Fig. 2 CNTs distribution pattern for three different FG-CNT nanocomposites

Table 1 Value of parameters [17]

Property	Value
Modulus of elasticity of CNT, $\mathbf{E_t}$	1000 GPa
Poisson's ratio of CNT, $\boldsymbol{\nu_t}$	0.27
Modulus of elasticity of aluminum, $\mathbf{E_m}$	7000 MPa
Poisson's ration of aluminum, $\boldsymbol{\nu_m}$	0.23

be defect-free and perfectly bonded with the matrix material. Material properties for Al and the CNTs are obtained from published literature [17] as shown in Table 1. The indenter for the present analysis is modeled as a rigid hemisphere with a 10 nm radius. Model boundary conditions are set to restrict node movements appropriately, ensuring a proper analysis. The indentation process is simulated by lowering the indenter by 0.3 nm, followed by a gradual withdrawal until it is fully detached from the nanocomposite (simulating the unloading phase of the contact). Frictionless contact is considered between the rigid indenter and the nanocomposite and the generation of the contact pair involves the use of the Lagrangian contact algorithm. Choice of proper elements to simulate the contact is an important aspect. Solid 187 elements are employed for meshing, along with CONTA174 contact elements forming a pair with TARGE170 elements on the rigid indenter surface. The meshed model of the contact interface is portrayed in Fig. 1. Mesh refinement is done near the contact zone for accuracy and a convergence analysis confirms the optimal mesh configuration with 285,742 elements.

3 Validation Study

Model validation is one of the primary and essential parts of the numerical study. The validation process is accomplished based on the results from the present model which is adapted to analyze a somewhat similar system for which numerical/experimental results are available in the literature. However, based on the extensive literature survey it is established that no work has been published on spherical indentation contact analysis of functionally graded CNT nanocomposite using a 3D model. In

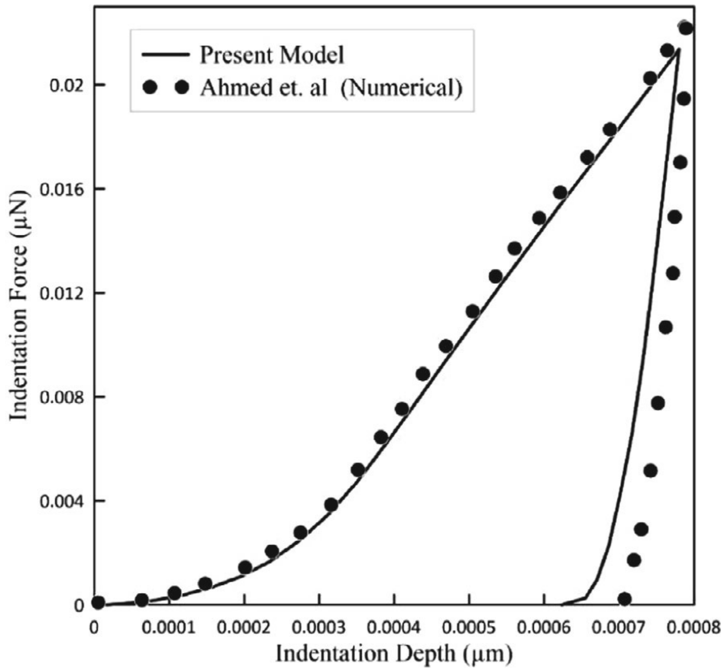

Fig. 3 Validation: comparative plot of indentation force versus indentation depth

the present scenario, the model is validated by carrying out a comparison with results of CNT-reinforced Al nanocomposite in the 2D domain published by Ahmed et al. [17].

The material model is adopted from the model described in the literature published by Ahmed et al. [17]. The analysis is carried out for a nanocomposite where CNTs are uniformly distributed within the matrix. Dimensions of the nanocomposite block are considered as 10 nm × 10 nm and CNT wall thickness of 0.168 nm is chosen to maintain parity with the original model. A Berkovic indenter is used for the indentation process and results are extracted under loading and unloading conditions. The contact force versus indentation depth results of the published and present model are plotted to compare as shown in Fig. 3. Satisfactory agreement was found between the two sets of data as the curves follow the same pattern. This comparison can be treated as validation of the present model.

4 Finite Element Analysis Results

The spherical indenter interacts with a FG-CNT with the specified CNT distribution. The indenter is initially lowered to a predetermined depth, causing deformation and creating a finite contact area. The model assumes a pure slip condition to eliminate friction effects on contact area and force generation during loading. The material properties beneath the indented face significantly influence the behavior of the system. Initially, contact occurs between aluminum (Al) and the rigid body, but as indentation depth increases, the pronounced effect of carbon nanotubes (CNTs) becomes evident.

Figure 4 illustrates the variation of contact force against indentation depth for different CNT distribution patterns (refer Fig. 2). The plot indicates that variation of contact force (corresponding to the three different patterns) is minimal at lower indentation depths but becomes more prominent with increasing indentation depth. As the indenter comes in contact with the matrix material only and as long as the depth of indentation is low, presence of the nanotubes has low influence. Once the indentation depth increases the CNTs start to affect the response of the material. If a small upper band near the surface is taken into consideration, the number of CNTs (consequently the volume fraction of CNTs in comparison to matrix material) present in this layer plays a major role in determining the response curve. The volume percentage of CNTs increases from lower to higher near the contact zone for the FG-Λ, FG-UD, and FG-V patterns. This increase in volume percentages can be correlated with enhanced stiffness and yield stress of the nanocomposite and as evidenced by the results of contact force from the present model. Moreover, the contact force difference becomes more pronounced at higher indentation depths, highlighting CNTs' resistance to indentation due to their higher strength compared to the matrix material (Al).

Figure 5 presents the relationship between the indentation depth of the rigid spherical indenter and the contact area of the FG-CNT nanocomposite block for different CNT distribution patterns. The indenter undergoes downward loading, reaching an indentation depth of 0.003 μm and subsequent and upward unloading. A similar trend is observed for the contact area as in the case of indentation depth versus contact force plot. However, beyond a specific indentation depth of 0.0018 μm (approximately), FG-UD and FG-V curves intersect. It may be due to the presence of varying number of CNTs present in the zone near the surface.

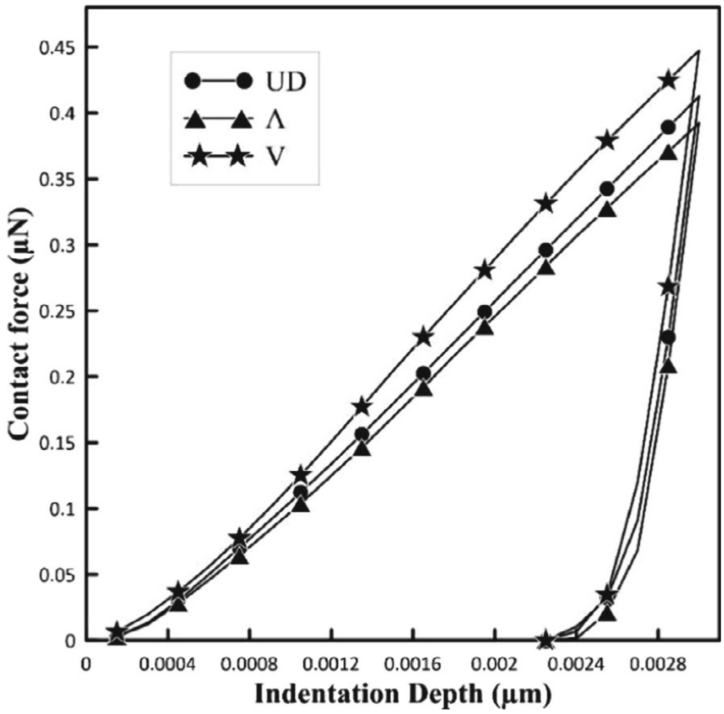

Fig. 4 Indentation depth versus contact force plots for different CNTs distribution pattern

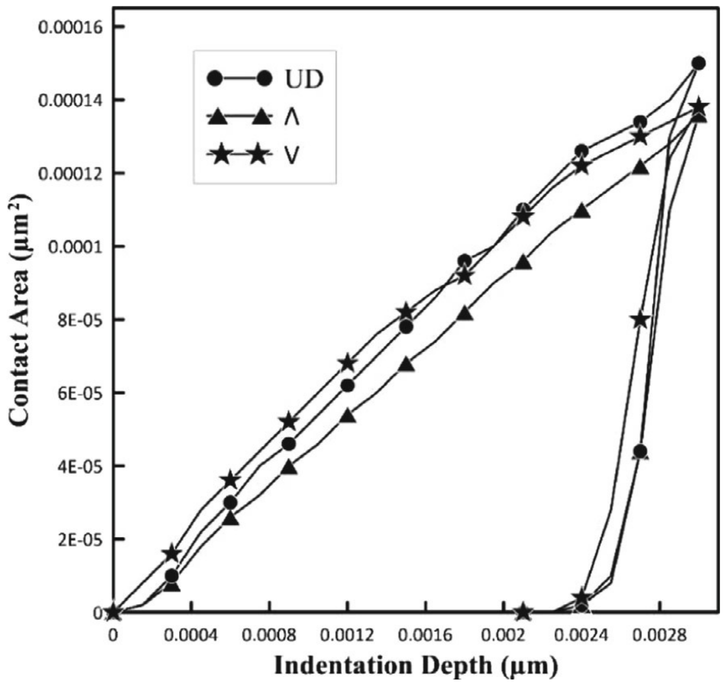

Fig. 5 Indentation depth versus contact area plots for different CNTs distribution pattern

4.1 Analysis of Stresses

The analysis of stress distributions is a crucial aspect of contact analysis. Contour plots illustrating von Mises stress distributions, with varying patterns of CNT distribution, are presented in Figs. 6 and 7. The plots are divided into two columns: one for the entire FG-CNT nanocomposite (Figs. 6(i) and 7(i)) and the other for the matrix material (Al) alone (Figs. 6(ii) and 7(ii)), providing a comprehensive comparison.

The contour plots of the FG-CNT's average von Mises stress distribution at the end of loading with change in CNT distribution pattern are displayed in Fig. 6(a) to (c). The figures make it evident that the UD pattern experiences the highest average von Mises stress at the end of loading because there are fewer highly affected CNTs near the contact zone with respect to others. So, it can be inferred that in the number of CNTs in a zone immediately below and in the vicinity of contact is an extremely important parameter. Presence of fewer numbers of highly affected CNTs leads to larger stresses as observed in the figure of contour plots of only Al at the end of the loading stage (Fig. 6(a)–(i)). It is also observed that the generated stresses are dispersed over a small volume of the matrix material. On the other hand, FG-V nanocomposite exhibits a lowest peak stress within the matrix. But, zone of generated stress is spread over a larger volume—penetrating to a greater depth and spread over a larger surface area.

Across all contour plots, considering loading and unloading stages with different CNT distribution patterns, it is evident that the highest von Mises stress occurs in the UD pattern compared to others. As a matter of fact, FG-UD nanocomposite experiences higher stress at the conclusion of both loading and unloading stages.

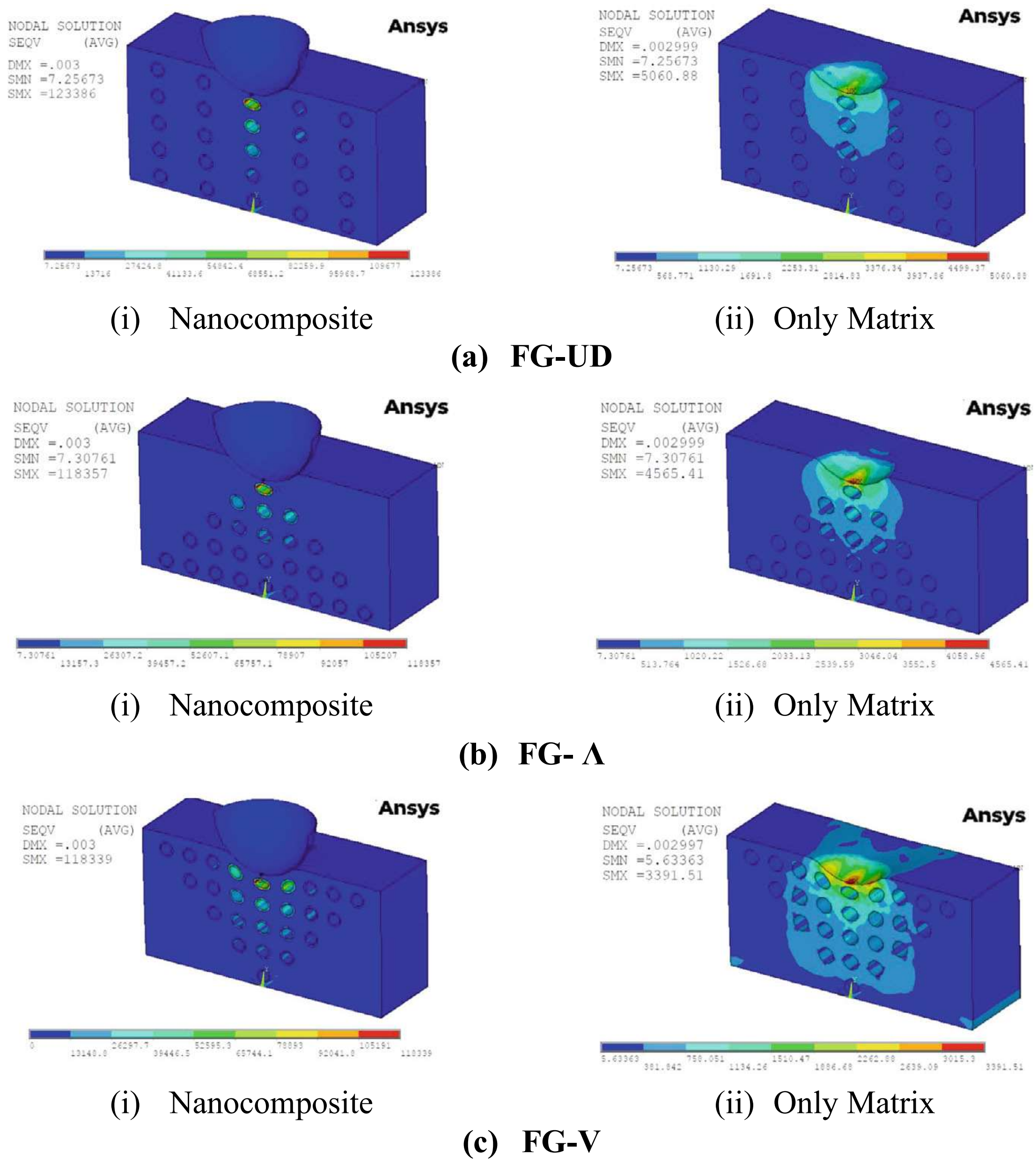

Fig. 6 Contour plot of average von Mises stresses for different FG-CNT (FG-UD, FG-V, and FG-V) after loading to an indentation depth of 0.003 μm

In Fig. 7, contour plots of residual von Mises stress for three distinct FG-CNTs, unloaded from an indentation depth of 0.003 μm, are displayed in (a) to (c). The observed trend of the residual von Mises stress distribution mirrors that of the average von Mises stress at the end of the loading stage. Peak stress occurs where the material is most displaced along the direction of indentation, with highly stressed points observed in CNTs near the contact zone. The highest stressed zones are typically located beneath the contact area, a result of plastic yielding in the material during deformation.

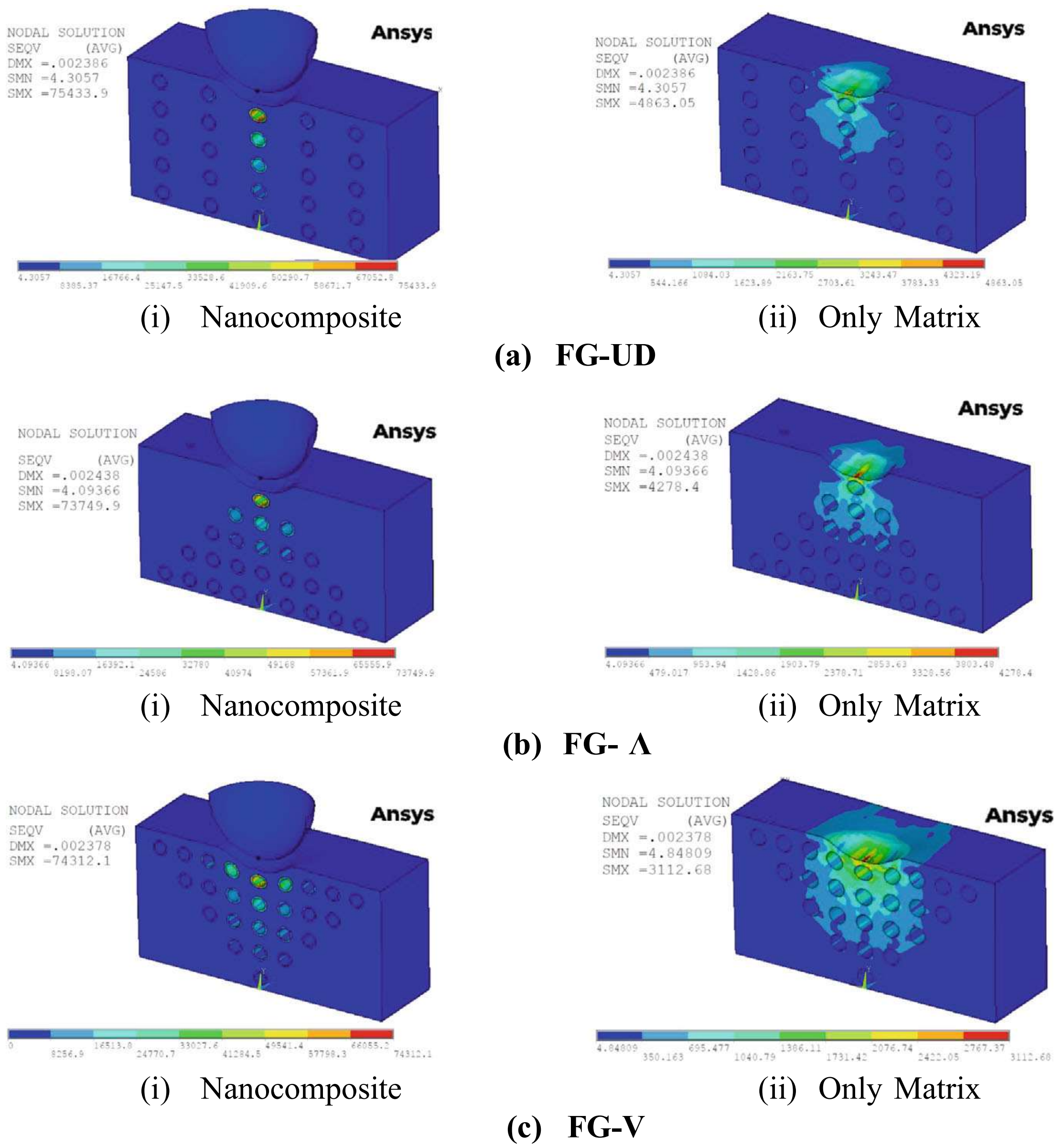

Fig. 7 Contour plot of residual von Mises stresses for different FG-CNT (FG-UD, FG-V, and FG-V) after completion unloading from an indentation depth 0.003 μm

4.2 Analysis of Deformation

In this section, several aspects of FG-CNT deformation are examined with variations in the pattern of CNT distribution of the nanocomposite.

Fig. 8(a) and (b) depict the *y*-directional (vertical) displacement of nodes along the line in the bisection on the contact surface of the nanocomposite. Figure 8(a) shows how the nodes' position varies at the end of loading, influenced by different CNT distribution patterns in FG-CNT. In a magnified view, higher sink-in is observed for FG-UD during loading and lower for FG-V near the contact zone. This is attributed to the soft properties of Al and CNT deformation causing material flow to fill the void

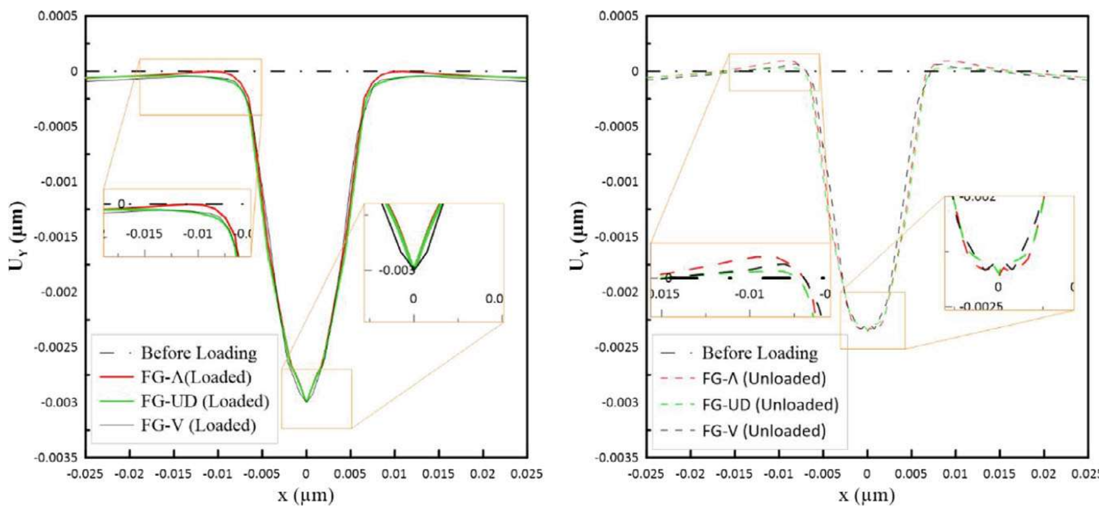

(a) Loading (b) Unloading

Fig. 8 Nodal displacement in *y*-direction at the line of contact between the bisectional plane and plane of contact—(**a**) Loading (to an indentation depth of 0.003 μm) and (**b**) Unloading (from an indentation depth of 0.003 μm) for different FG-CNT

left by the deformed CNTs. It results in compression of the matrix material beneath the contact zone. The average von Mises contour plot in Fig. 6 and the increased nanotube deformation near the contact zone, especially influenced by FG-UD, may be linked to the observed sink-in behavior during loading. At the end of unloading in Fig. 8(b), the topography reveals a pile-up phenomenon, more pronounced for FG-V due to lower average von Mises stress at the end of loading and lower residual von Mises stress (Fig. 7). This pile-up behavior aligns with findings in experimental and numerical investigations of pure Al substrate indentation [18, 19]. Permanent deformation and the spring-back effect are influenced by residual von Mises stress, explaining FG-V's larger pile-up behavior.

The contour plots of *y*-direction nodal displacement at the end of the loading and unloading stages are shown in Figs. 9 and 10, respectively. The largest displacement in the *y*-direction is observed at the point of contact along the line of bisection. The contour plot of *y*-directional displacement shows that residual deformation follows the same pattern as mentioned in the section on residual stress at the end of unloading.

5 Conclusions

On the ANSYS platform, FEM is used to simulate indentation contact between FG-CNT nanocomposite and a rigid spherical indenter during loading and unloading phases. Variation of distribution pattern of embedded CNTs are considered in order to implement a functional gradation of properties along the depth of the nanocomposite. For the present study, three different distribution patterns are considered. To achieve accurate results, appropriate elements are utilized for the contact interface as well

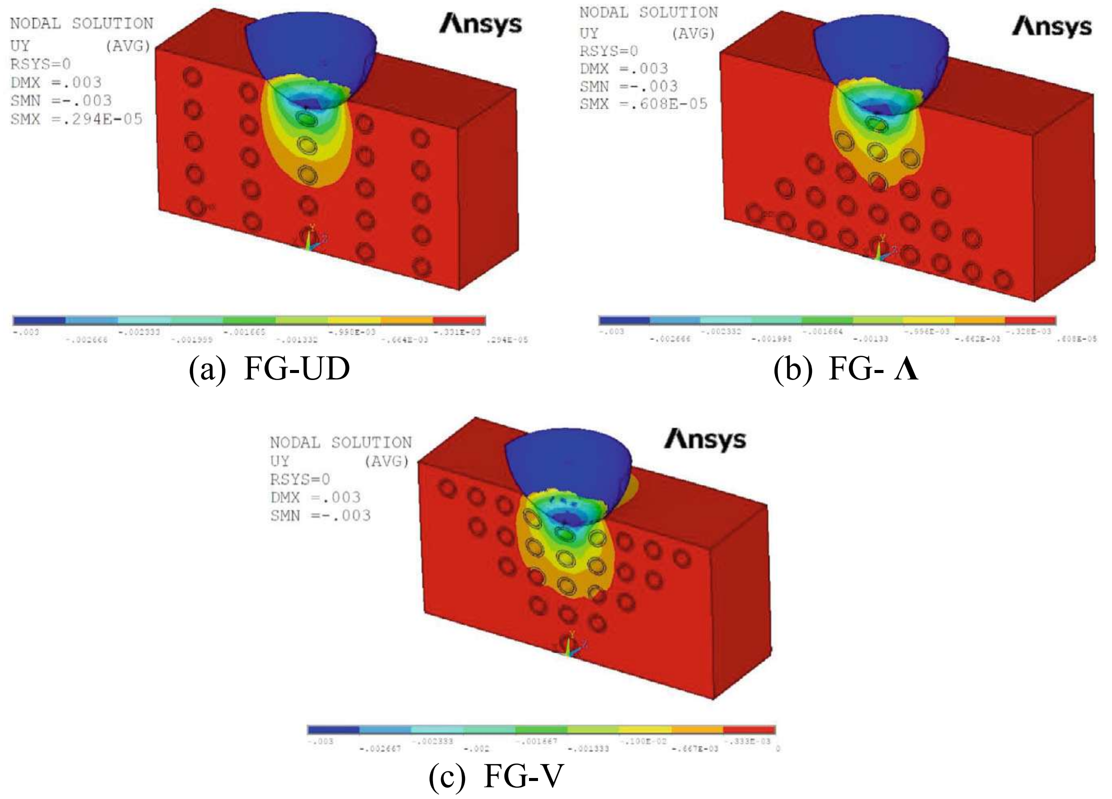

Fig. 9 Contour plot of *y*-direction nodal displacement at an indentation depth of 0.003 μm at the completion of the loading stage with different FG-CNT

as the bulk material. To determine suitable number of elements for the analysis, a convergence study is also carried out. Prior to analysis, the right boundary conditions are chosen and the developed model is validated using relevant published literature. Understanding the impact of various FG distributions of CNTs in the contact domain is the goal of the study as already discussed in the introduction section. It should be mentioned here that no published literature is available for contact analysis of FG-CNTs and hence, the results of the current study can act as benchmark in the relevant domain. Different contact properties, such as contact force, contact area, average von Mises stresses residual von Mises stresses, and deformation behavior are presented and analyzed. The following observations and conclusions could be drawn from the results:

- Compared to uniformly distributed FG-CNT, the contact force rises for FG-V and falls for FG-Λ. This effect may be brought on by an increase in CNT density at the contact surface, which causes a greater volume of the nanocomposite to be damaged during loading which may give a greater resistive force. A similar trend is also observed in the case of the contact area.
- Interestingly, the FG-UD nanocomposite creates the highest average von Mises stress because there are less significantly affected CNTs in the nanocomposite materials and more matrix material is displaced during loading. High residual

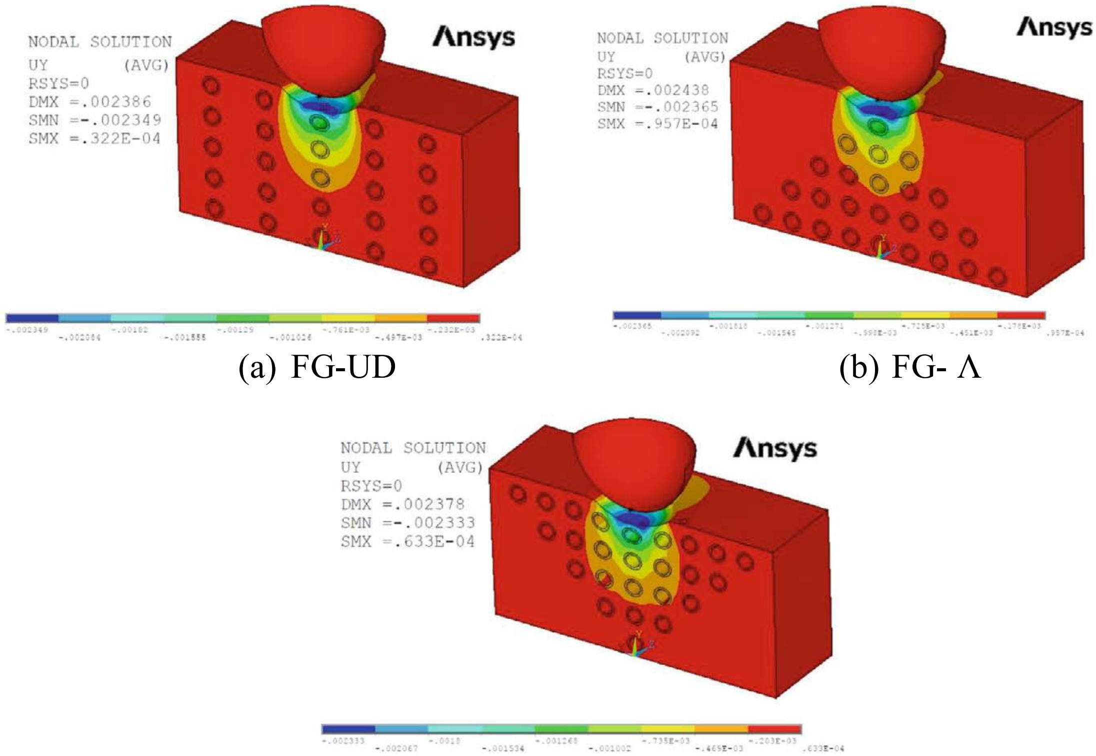

(a) FG-UD (b) FG- Λ

(c) FG-V

Fig. 10 Contour plot of *y*-direction nodal displacement at the end of unloading from an indentation depth of 0.003 μm with varied FG-CNT

von Mises stress develops at the end of the unloading stage, leading to permanent deformation in the indentation zone.

- Sink-in behavior is observed at the end of loading, except FG-Λ, and pile-up is also observed at the end of unloading for all the nanocomposites.
- Based on the findings, it can be said that FG-V has better contact properties than FG-UD and that FG-Λ nanocomposite has poorer contact behavior.

References

1. Zhang Y, Sun MJ, Zhang D (2012) Designing functionally graded materials with superior load-bearing properties. Acta Biomater 8(3):1101–1108
2. Suresh S (2001) Graded materials for resistance to contact deformation and damage. Science 292(5526):2447–2451
3. Shen HS, Zhang CL (2010) Thermal buckling and postbuckling behavior of functionally graded carbon nanotube-reinforced composite plates. Mater Des 31(7):3403–3411
4. Shen HS, Xiang Y (2013) Nonlinear analysis of nanotube-reinforced composite beams resting on elastic foundations in thermal environments. Eng Struct 56:698–708
5. Shiau LC, Kuo SY (2004) Thermal buckling of composite sandwich plates. Mech Based Des Struct Mach 32(1):57–72

6. Zhu P, Lei ZX, Liew KM (2012) Static and free vibration analyses of carbon nanotube-reinforced composite plates using finite element method with first order shear deformation plate theory. Compos Struct 94(4):1450–1460
7. Shen HS (2012) Thermal buckling and postbuckling behavior of functionally graded carbon nanotube-reinforced composite cylindrical shells. Compos B Eng 43(3):1030–1038
8. Yas MH, Samadi N (2012) Free vibrations and buckling analysis of carbon nanotube-reinforced composite Timoshenko beams on elastic foundation. Int J Press Vessels Pip 98:119–128
9. Mehrabadi SJ, Aragh BS, Khoshkhahesh V, Taherpour A (2012) Mechanical buckling of nanocomposite rectangular plate reinforced by aligned and straight single-walled carbon nanotubes. Compos B Eng 43(4):2031–2040
10. Kerur SB, Ghosh A (2011) Active control of geometrically non-linear transient response of smart laminated composite plate integrated with AFC actuator and PVDF sensor. J Intell Mater Syst Struct 22(11):1149–1160
11. Bhadra R, Jana T, Mitra A, Sahoo P (2023) Effect of CNT radius on flattening contact behaviour of CNT-Al nanocomposite: a numerical approch. Rep Mech Eng 4(1):121–130
12. Bhadra R, Jana T, Mitra A, Sahoo P (2023) Finite element based indentation contact analysis of SWCNT nano-composite. Proc Inst Mech Eng, Part C: J Mech Eng Sci 09544062231169138
13. Bhadra R, Jana T, Mitra A, Sahoo P (2022) Flattening cylindrical contact analysis of single walled carbon nanotube (SWCNT) nanocomposite. Int J Surf Eng Interdisc Mater Sci (IJSEIMS) 10(1):1–22
14. Baltacıoğlu AK, Civalek Ö (2018) Vibration analysis of circular cylindrical panels with CNT reinforced and FGM composites. Compos Struct 202:374–388
15. Yadav A, Bhardwaj G, Godara RK (2022) Thermally induced fracture analysis of CNT reinforced FG structures with multiple discontinuities using XIGA. Eng Fract Mech 275:108822
16. Lei ZX, Liew KM, Yu JL (2013) Free vibration analysis of functionally graded carbon nanotube-reinforced composite cylindrical panels. Int J Mater Sci 1:36–40
17. Ahmed KS, Ibrahim I, Keng AK (2020) Advanced nanoindentation simulations for carbon nanotube reinforced nanocomposites. Heliyon 6(8)
18. Moharrami N, Bull SJ (2014) A comparison of nanoindentation pile-up in bulk materials and thin films. Thin Solid Films 572:189–199
19. Taljat B, Pharr GM (2004) Development of pile-up during spherical indentation of elastic–plastic solids. Int J Solids Struct 41(14):3891–3904